

# Drying and Crystallization of Evaporating Sodium Nitrate Aerosol Droplets

F. K. A. Gregson,\* J. F. Robinson, R. E. H. Miles, C. P. Royall, and J. P. Reid

Cite This: *J. Phys. Chem. B* 2020, 124, 6024–6036

Read Online

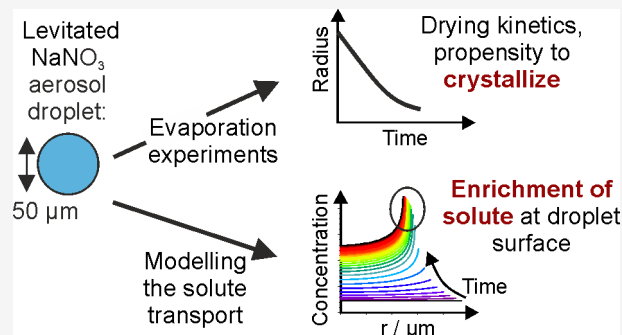
ACCESS |

Metrics &amp; More

Article Recommendations

Supporting Information

**ABSTRACT:** The evaporation of liquid solution droplets and solute crystallization can be highly complex and is an important problem, particularly in spray drying where powdered products are produced from sprayed liquid droplets, such as in the food or pharmaceutical industries. In this work, we study the relationship between the evaporation rates of single levitated  $\text{NaNO}_3$  droplets under varying environmental conditions and the propensity for nucleation of  $\text{NaNO}_3$  crystals. We use a combination of an electrodynamic balance to study single-droplet evaporation kinetics, SEM imaging of dried particles, and modeling of the internal solute distribution inside a drying droplet. We show that the aqueous  $\text{NaNO}_3$  droplets exhibit broad distributions in the time that crystal nucleation is observed, droplet to droplet. The distribution of nucleation time is dependent upon environmental conditions such as the drying temperature, relative humidity (RH), and solute concentration. Even when evaporating in 0% RH, some droplets do not nucleate crystals in the time taken for all water to evaporate and dry to form an amorphous particle. We believe that this interplay between crystalline or amorphous particle formation is a result of the viscosity of aqueous  $\text{NaNO}_3$  solutions, which rises by several orders of magnitude as the concentration increases. We show that for droplets with an initial radius of  $\sim 25 \mu\text{m}$  the propensity for aqueous  $\text{NaNO}_3$  droplets to nucleate crystals upon drying increases with a decreasing RH and increases with an increasing temperature in the range 278–306 K. This work demonstrates the importance of the drying kinetics on the propensity of evaporating droplets to nucleate crystals.



flows.<sup>16,17</sup> Hence, single particle techniques are valuable for studying crystallization behavior of formulations in a controlled fashion.<sup>18</sup> For spray drying applications, understanding the propensity for a drying aerosol droplet to crystallize under different conditions is important. In the broader sense, an aerosol droplet of pure components, in the absence of any surface able to induce heterogeneous nucleation, can facilitate study of the homogeneous nucleation process. Homogeneous nucleation of crystals out of a solution typically only occurs at a high degree of supersaturation, which is not accessible in the bulk phase. Thus, aerosol studies on homogeneous nucleation are important for validating theories of nucleation.<sup>19,20</sup>

## I. INTRODUCTION

The formation of solid particles from evaporating liquid droplets is an important process across a broad range of industries and application areas. The design and fabrication of particles by using spray drying has attracted much attention in recent years with a goal to improve the reproducibility and uniformity of the particles formed and the range of situations in which it can be applied. Particle size, morphology, size distribution, and degree of crystallinity have been shown to be affected by changes to the droplet processing conditions such as solvent,<sup>1,2</sup> temperature,<sup>3–5</sup> starting pH,<sup>6,7</sup> and inert additives to the feed solution.<sup>8–10</sup>

Particles of amorphous material, rather than crystalline, are often desirable in drug delivery applications because of their solubility and the bioavailability of active ingredients.<sup>11,12</sup> In contrast, crystalline products may be more appropriate for some applications as they often offer a higher degree of stability in long-term storage with particles stable to phase changes.<sup>13–15</sup> Whichever phase is more desirable for the application, the ability to predict and control the presence of amorphous or crystalline content in a product is highly beneficial.

In an industrial spray drier it can be difficult to observe crystallization directly due to the speed of the process, the vast quantity of droplets present, and the highly dynamic circulating

Classical nucleation theory (CNT) is commonly used to understand nucleation of crystals out of solution. Crystal nucleation is governed by the change in Gibbs free energy ( $\Delta G$ ) between solution and crystal phase. In CNT we express  $\Delta G_{\text{cryst}}$  as the competition between the free energy loss of

Received: May 7, 2020

Revised: June 16, 2020

Published: June 22, 2020



forming a cluster of solute and the free energy gain caused by the creation of a phase boundary between the cluster and the solution.<sup>20–22</sup>

$$\Delta G_{\text{cryst}}(n) = -n\Delta\mu + \gamma A \quad (1)$$

where  $n$  is the number of solute molecules in a cluster,  $\Delta\mu$  is the chemical potential change, per molecule, between solution and crystal, and  $\gamma$  is the surface tension between a cluster and the surrounding solution.  $A$  is related to the dimensions of the cluster and is proportional to  $n^{2/3}$ , so the function in eq 1 goes through a maximum,  $\Delta G_{\text{cryst}}^*$  at a critical cluster size  $n^*$ , after which  $\Delta G_{\text{cryst}}$  decreases monotonically with  $n$  leading to spontaneous crystal growth.

The nucleation rate of crystals out of solution per unit volume per unit time,  $J$ , is typically expressed in the form of an Arrhenius equation:

$$J = K \exp\left[\frac{-\Delta G^*}{k_{\text{B}}T}\right] \quad (2)$$

where  $K$  is the pre-exponential factor taking kinetic considerations into account such as diffusive transport,  $k_{\text{B}}$  is the Boltzmann constant, and  $T$  is the equilibrium temperature.

While classical nucleation theory has been shown to be useful in interpreting nucleation data,<sup>23</sup> there are many underlying assumptions to simplify the theory that are unlikely to hold. CNT assumes that the crystal nucleus has identical macroscopic properties to the equilibrium crystalline phase, such as density, surface free energy, and structure, as well as the assumption that the interface between the nucleus and surrounding solution is a sharp, spherical boundary. In addition, CNT often fails to explain the apparent absence of a nucleation barrier at very high supersaturations,<sup>24</sup> with such concentrations being prevalent in the aerosol phase.

Nucleation of crystals out of solution in an aerosol droplet is often described in terms of an absolute “efflorescence RH” (ERH). If a liquid aerosol particle is dried into an environment of continuously decreasing RH, it will continue to lose water and will enter a regime of solute supersaturation. The ERH is the lowest RH at which the droplet can remain as a supersaturated liquid before crystallizing into a microparticle. If the same microparticle is then exposed to an increasing humidity, it will take up water and dissolve into an aqueous solution droplet only at a certain RH known as the deliquescence RH (DRH). This efflorescence–deliquescence cycle is characteristic to inorganic aerosol droplets.<sup>25</sup> Typically, if an inorganic aqueous-solution droplet is dried into a lower RH than the ERH, then crystallization will be observed. This has been shown to be reproducible across large populations of NaCl aerosol droplets, with a very narrow distribution in the time at which crystallization is observed to occur as droplets are dried.<sup>26</sup> Thus, crystal nucleation in inorganic aerosol droplets is often assumed to be a spontaneous process. Few experimental techniques currently exist for studying the kinetics of nucleation *in situ* in aerosol droplets,<sup>27</sup> and as such, crystallization of aerosol is typically only described in terms of an ERH.

In this study, we investigate the nucleation propensity upon evaporation of aqueous sodium nitrate droplets. Sodium nitrate was chosen as a system to study because the hygroscopicity has been well-defined by previous experiments as well as models,<sup>28,29</sup> making its concentration at varying RHs well characterized, but it does not exhibit a well-defined ERH,

suggesting interesting nucleation behavior. In addition, the bulk solubility limit of NaNO<sub>3</sub> shows a strong dependence upon the temperature.<sup>30</sup> Efflorescence has been observed over a range of published studies to occur at RHs in the range 0.05%–40%. Ghorai and Tavanski<sup>31</sup> reported the RH at which NaNO<sub>3</sub> crystallized as 35% measured using X-ray spectromicroscopy. Tang and Munkelwitz<sup>32</sup> levitated NaNO<sub>3</sub> droplets in an electrodynamic balance and evaporated them into a range of RHs and observed efflorescence in individual droplets between 0.05% and 30% RH. Lee et al.<sup>33</sup> supported micrometer-sized NaNO<sub>3</sub> droplets on a TEM grid and studied their propensity to crystallize. They reported different types of droplets, each of which had different efflorescence and deliquescence RHs (between 18–45% and 73–75%, respectively), with some droplets not appearing to undergo either process. Likewise, in optical tweezers, NaNO<sub>3</sub> droplets have been evaporated slowly to as low as 10% RH without crystallization occurring, showing that a liquid droplet at such high levels of solute supersaturation can still remain in equilibrium with the gas-phase RH.<sup>27</sup>

In this work, our goal is to highlight the variability in nucleation behavior in large populations of individual aerosol droplets, which exhibit stochastic behavior. We will demonstrate that the nucleation of NaNO<sub>3</sub> cannot be described by an ERH and by a thermodynamic critical supersaturation. By observing distributions of nucleation events across many different drying conditions, we show that the drying kinetics lead to different outcomes in the competition between crystalline and amorphous particle formation, which explains the inconsistency in the reported ERH in the above studies. A combination of EDB measurements, SEM imaging of dried particles, and a numerical model is used. In section II, we describe the experimental techniques for isolating single aerosol solution droplets and determining the particle size and phase state throughout drying. In section III we show results of the evaporation and nucleation kinetics of NaNO<sub>3</sub> solution droplets under different environmental conditions, such as under varying RHs and temperatures. We use an accompanying model to study the evolving concentration profiles inside an evaporating NaNO<sub>3</sub> droplet to explain the observed nucleation kinetics.

## II. EXPERIMENTAL TECHNIQUES AND MODELING

**II.a. Electrodynamic Balance.** The evaporation kinetics of NaNO<sub>3</sub> droplets are measured by using the comparative kinetics electrodynamic balance (CK-EDB). In all experiments, HPLC grade water, analytical grade NaNO<sub>3</sub> (Fisher-Scientific), and BioXtra ≥99.5% NaCl (Sigma-Aldrich) were used. The EDB instrument has been discussed in a previous publication<sup>34</sup> and so will only be briefly outlined here. A single droplet of known composition is produced by using a droplet-on-demand generator (MicroFab) and injected into the CK-EDB instrument. The initial droplet size is typically  $\sim 25 \pm 0.08 \mu\text{m}$ . The droplet is charged on generation ( $\sim fC$ , e.g., from an ion imbalance) by an induction electrode. An AC voltage is applied to a pair of upper and lower concentric cylindrical electrodes, mounted vertically opposite one another, such that the charged droplet becomes trapped in the electrodynamic field at the center of the instrument. An additional DC voltage is applied to the bottom electrode only to counteract the gravitational force acting on the droplet. The temperature in the trapping chamber is controllable within the range 273–323 K by a circulating flow of ethylene glycol coolant that passes across

the electrodes and measured with a thermocouple (National Instruments) The RH in the CK-EDB can be controlled by adjusting the ratio between dry and wet nitrogen in a gas flow (RH range 0–100%) that is applied across the droplet at a rate of  $0.03 \text{ m s}^{-1}$ . The instrument has two gas flows with the independent control of RH of each: one flowing upward through the lower electrode (lower flow) and one flowing downward through the upper electrode (upper flow). By use of mass-flow controllers (MKS), a rapid switch (within  $\sim 0.1 \text{ s}$ ) can be made between which gas flow is the dominant one and therefore the one experienced by the particles. The approximate RH in the chamber is determined by using the ratio of dry to wet nitrogen flows set on the mass flow controllers, with an accuracy of  $\sim \pm 2\%$ . The wet and dry gas flows are mixed at 293 K, so all experiments wherein the RH is varied are performed at 293 K. If the temperature is varied, only the dry  $\text{N}_2$  gas flow is used to maintain the RH at 0%.

**II.b. Sizing the Droplet and Analysis of the Particle Phase State.** The trapped droplet in the EDB is illuminated with a 532 nm continuous-wave laser (Laser Quantum, Ventus, UK), and the scattering pattern produced by the droplet takes the form of interference fringes (phase function). The phase function (PF) is recorded by a CCD camera (CMOS, Thorlabs) placed at  $45^\circ$  to the propagation direction of the beam, with an angular collection range of  $\sim 24^\circ$ . The angular separation between the interference fringes,  $\Delta\theta$ , can be used to calculate the droplet radius,  $r$ , by using the geometric optics approximation to Mie theory:

$$r = \frac{\lambda}{\Delta\theta} \left[ \cos\left(\frac{\theta}{2}\right) + \frac{m \sin\left(\frac{\theta}{2}\right)}{\sqrt{1 + m^2 - 2m \cos\left(\frac{\theta}{2}\right)}} \right]^{-1} \quad (3)$$

where  $\lambda$  is the laser wavelength,  $\theta$  is the central viewing angle, and  $m$  is the refractive index of the droplet. This approximation can determine the radius to an accuracy of  $\pm 100 \text{ nm}$ .

The angular intensity profile of the elastic light scattering can be used to infer the trapped particle structure by using the algorithm outlined in Haddrell et al.<sup>35</sup> The structure can be continuously monitored throughout the evaporation process, with four distinct morphologies identifiable: homogeneous and spherical (i.e., a liquid aerosol droplet); nonspherical and inhomogeneous (e.g., like a crystalline salt particle); a core-shell particle (i.e., phase-separated surface shell and inner core); and a droplet containing inclusions. In the latter case, the droplet shape is overall spherical, but there are internal areas of inhomogeneity (i.e., inclusions) that disrupt the light scattering. The algorithm fits functions to the light scattering phase function and, in a droplet on the order of  $20 \mu\text{m}$ , can reproducibly detect internal inclusions that are of radius  $>40 \text{ nm}$  down to a percent volume of inclusions of 0.05%.<sup>35</sup> For inclusions of  $40 \text{ nm}$ , 0.05 vol % corresponds to a quantity of 62500 detectable inclusions in a  $20 \mu\text{m}$  droplet.

When the droplet is first produced, it scatters the laser light in the form of a regular phase function, such that an accurate value of the radius can be calculated. If nucleation occurs in a droplet, the scattering pattern will show crystallinity or inclusions; hence, the radius can no longer be determined accurately by the EDB instrument. This point in time is thus recorded as the “nucleation time”, and the time sensitivity is the minimum interval at which the EDB records the PF, which is  $\sim 0.01 \text{ s}$ . This method to detect efflorescence in aerosol

droplets was previously used to study the nucleation in aqueous NaCl droplets.<sup>26,36</sup> An example of the light scattering from a homogeneous droplet or a crystalline droplet is shown in Figure S1 of the Supporting Information. If crystals nucleate, they must grow to a minimum size to be detectable by the light scattering, which is  $\sim 0.05\%$  the volume of the droplet. The induction time is defined as the time period from the moment a solution becomes supersaturated until the instant that crystals are detected.<sup>37</sup> For the droplets in the EDB, the time scale for the growth period of a crystal nucleus before it is detected is assumed to be small and thus a negligible contribution to the induction time.

In this work, droplets of aqueous  $\text{NaNO}_3$  were evaporated within the EDB, and the kinetics of evaporation and the propensity to crystallize were measured across a range of RHs, temperatures, and initial feed concentrations.

**II.c. Collection of Dried Particles and Imaging.** To investigate the morphology of dried  $\text{NaNO}_3$  particles, a falling droplet column instrument was used because dried particles cannot be collected from the EDB instrument. In parallel measurements under analogous drying conditions to those used in the EDB, droplets of  $\text{NaNO}_3$  are dried in the column, and the dried particles collected on a glass slide as the substrate.  $\text{NaNO}_3$  droplets of  $\sim 25 \mu\text{m}$  in radius are produced at a rate of 10 Hz by using the same dispensers as in the CK-EDB measurements (MicroFab) and are directed in a falling chain of droplets down a vertically mounted glass column of 50 cm in length. The RH in the column is maintained at 0% by flowing dry  $\text{N}_2$  gas down through the column, and the temperature is maintained at  $20^\circ \text{C}$  by using a heating wire wrapped around the column with a calibrated temperature probe. A vertically propagated laser ( $\lambda = 532 \text{ nm}$ ) is aligned directly up the column to image the falling chain of droplets and to ensure that there is sufficient fall time for the liquid droplets to dry into solid particles. The dried particles collected on a glass substrate are imaged by using a scanning electron microscope (Jeol IT300 SEM). A silver coating of  $\sim 15 \text{ nm}$  is applied to the particles and substrate, prior to imaging (sputter coater, Agar Scientific). The SEM imaging settings are a 15 mm working distance, 15.0 kV acceleration voltage, and a magnification of  $100\times$ – $2000\times$ . A schematic image of the falling droplet column instrument can be found in the Supporting Information (Figure S2).

**II.d. Modeling of Internal Concentration Profiles.** The concentration of solute at different radial points within an evaporating aqueous  $\text{NaNO}_3$  droplet is calculated by using a numerical model, outlined in detail in previous publications.<sup>26,38</sup> We consider the droplet as a series of concentric radial shells (of width  $\sim 20 \text{ nm}$ ) with a moving boundary. The evaporation rate, which controls the rate of surface recession, assumes quasi-static vaporization:

$$\frac{dm}{dt} = 4\pi C \rho_v D_v R \ln(1 + B) \quad (4)$$

where  $\rho_v$  and  $D_v$  are the density and vapor diffusion coefficient of the vapor phase, respectively.  $R$  is the molar gas constant, and  $B$  is the Spalding number,<sup>38,39</sup> which relates to the difference in solvent concentration at the surface and in the gas phase.  $C$  is an empirical correction to give correct agreement with the experimental mass flux at short times. The fit between the modeled droplet radii and the experimental radii is compared in Figure S3. The solute concentration profile is obtained by numerically integrating the diffusional mixing

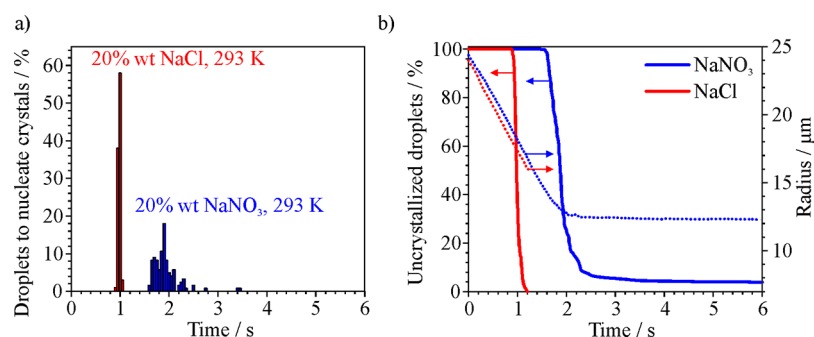


**Figure 1.** (a) Time at which nucleation is observed for a population of 100+ NaNO<sub>3</sub> droplets (20% w/w, starting radius  $\sim 24$   $\mu\text{m}$ ) as they evaporate in the CK-EDB in 0% RH and 293 K, compared to a population 20% NaCl droplets evaporating under the same conditions. (b) Data in (a) plotted as a percent of droplets that have not yet nucleated crystals as a function of time. The dotted lines show the radius evolution of the longest surviving NaNO<sub>3</sub> droplet and NaCl droplet in the data sets.

using finite difference methods via the standard diffusion equation:

$$\frac{\partial \rho_s}{\partial t} = \nabla(D_{\text{eff}} \nabla \rho_s) \quad (5)$$

where  $\rho_s$  is the concentration of solute and  $\nabla$  is the Laplace operator. For internal mass flux we assume Fick's law for diffusion which uses an effective binary diffusion coefficient,  $D_{\text{eff}}$ . Previous work using optical tweezers has determined the viscosity,  $\eta$ , of aqueous NaNO<sub>3</sub> solutions in the aerosol phase down to very low water activity.<sup>27</sup> Hence,  $D_{\text{eff}}$  is calculated via the Stokes–Einstein relation using a Stokes radius  $a$ :

$$D_{\text{eff}} = \frac{k_B T}{6\pi\eta a} \quad (6)$$

To determine  $a$ , we calibrated diffusion measurements from a molecular dynamics simulation<sup>39</sup> against the experimental viscosity data, which led to a value of  $a = 0.167$  nm for NaNO<sub>3</sub>. This is outlined in greater detail in our previous modeling paper.<sup>38</sup> The viscosity and diffusion coefficients are shown in Figure S4. The value of  $a$  used in the model lies between the literature values of the Stokes radius for Na<sup>+</sup> ions (0.184 nm)<sup>40</sup> and for NO<sub>3</sub><sup>-</sup> ions (0.129 nm).<sup>41</sup> As  $a$  is closer to the literature value of the Stokes radius of an Na<sup>+</sup> ion, the modeled concentration profiles in Figures 7–9 represent the concentration of Na<sup>+</sup>.

### III. RESULTS

**III.a. Comparison between NaNO<sub>3</sub> and NaCl Crystallization Behavior.** A series of droplets of aqueous NaNO<sub>3</sub> (20% w/w) are evaporated in the CK-EDB in dry N<sub>2</sub> at 293 K and held in the trap for a 10 s time window. For a population of 100+ droplets, the time at which nucleation is observed for each droplet is shown in the histogram in Figure 1a, grouped in 0.05 s time intervals. The data for NaNO<sub>3</sub> are compared with our previously published data for the observed nucleation of evaporating droplets containing aqueous NaCl (20% w/w).<sup>26</sup> In contrast to the NaCl data, 2.5% of NaNO<sub>3</sub> droplets do not crystallize within the 10 s experimental window despite appearing to lose all water and reach a constant size at 0% RH. Indeed, the phase function (PF) maintains regularly spaced fringes throughout the 10 s trapping period, implying that the droplet is homogeneous and spherical throughout.

In Figure 1b, we report the time dependence in the fraction of droplets still scattering light in a pattern consistent with a homogeneous and spherical droplet, i.e., the “decay” of

uncrystallized droplets. The shape of the decaying fraction remaining suggests that the crystallization is stochastic in nature. Owing to the very small initial droplet volume ( $\sim 60$  pL) and the high purity of both the NaNO<sub>3</sub> and water used, the chance of contaminants being present and inducing heterogeneous nucleation is low, and instead we assume all nucleation events herein to be homogeneous. We will return to a discussion of this assumption later.

The differences between the crystallization kinetics of a population of aqueous NaCl and aqueous NaNO<sub>3</sub> droplets are clear. Highly reproducible efflorescence behavior is observed for identical NaCl droplets generated in sequence, with crystallization occurring abruptly when the concentration of the solute at the surface of the droplets reaches a critical supersaturation of 2.04.<sup>26</sup> Figure 1b suggests a different form for the dependence of the nucleation rate of aqueous NaNO<sub>3</sub> droplets on supersaturation than observed for NaCl: there is no “critical supersaturation” which, when surpassed, leads to immediate nucleation. Rather, the NaNO<sub>3</sub> droplets enter a “nucleation window”<sup>42</sup> wherein there is opportunity for nucleation and crystallization to occur but which shows droplet-to-droplet variability.

For aqueous NaCl droplets evaporating in dry conditions, we previously presented simulations of the evolving internal concentration profiles and demonstrated that there is a high degree of solute enrichment at the surface of the droplets; the internal diffusional mixing cannot replenish the surface with water at the same rate that is evaporates.<sup>26</sup> Contrary to observations for aqueous sodium chloride droplets,<sup>43</sup> the viscosity of NaNO<sub>3</sub> has previously been shown to increase by more than 3 orders of magnitude as the water content decreases, up to the order of 1–10 Pa·s as it surpasses a mass fraction of solute of 0.9 and higher.<sup>27</sup> For aqueous NaNO<sub>3</sub> droplets evaporating into dry conditions, the rapid evaporation rate coupled with an increasing viscosity governed by the composition at the surface could lead to an even greater degree of solute enrichment than in the NaCl droplets. While a higher solute concentration should lead to a higher propensity to nucleate, the increase in viscosity with solute concentration may reduce the rate of nucleation by slowing ion mobility and the subsequent arrangement into a crystal nucleus.<sup>44</sup> These competing factors could lead to the shape of the decay curve in Figure 1b. It should be noted that the time of the “corner” in the blue curve of Figure 1b coincides approximately with the time of the radius equilibration. As water is continuously lost from the droplets throughout the initial evaporation, individual

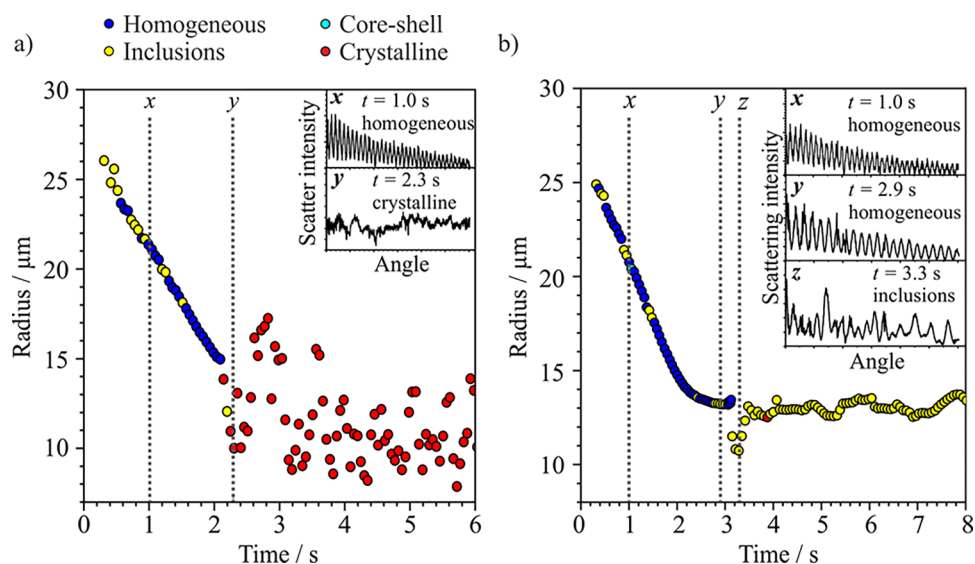


**Figure 2.** Evaporation profile of two individual aqueous droplets containing 20% (w/w)  $\text{NaNO}_3$ , evaporating into dry  $\text{N}_2$  at 293 K. The insets show the phase function of the light scattering at different times. The particle phase identified from the light scattering is indicated by the color of the points (blue = homogeneous and spherical, red = crystalline, and yellow = inclusions inside a spherical droplet). (a) A droplet that nucleates “early”, at  $\sim 2$  s, and has a largely crystalline phase function. (b) A “late” nucleating droplet at 3.2 s with a phase function indicating inclusions.

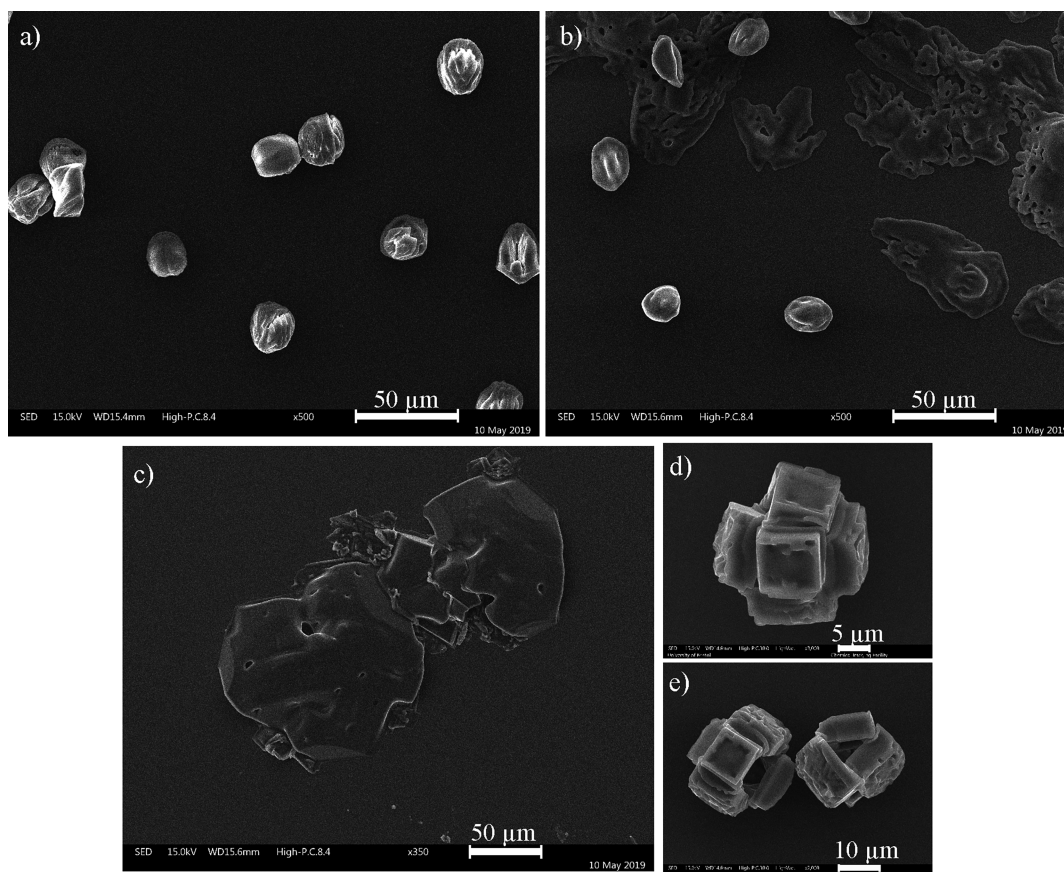


**Figure 3.** SEM images of  $\text{NaNO}_3$  particles collected on a glass side which were produced by evaporating aqueous 20% (w/w)  $\text{NaNO}_3$  droplets in dry  $\text{N}_2$  at 293 K in a falling droplet column. Storage conditions from the point of collection until the SEM imaging step were (a) in a 0% RH desiccator, (b) a 7 h period stored at 60% RH before being stored in a 0% desiccator, and (c) a 2 h period stored at 90% RH before being stored in a 0% desiccator. (d, e) SEM images of a  $\text{NaCl}$  particles from a sample collected from evaporating 20% (w/w) aqueous  $\text{NaCl}$  droplets in dry  $\text{N}_2$  at 318 K in a falling droplet column.

droplets within the population begin to nucleate crystals on a regular, if not predictable, basis. However, if nucleation has not yet occurred before the time that a droplet has almost lost all

water ( $\sim 2$  s into evaporation), the viscosity becomes so high that the chance of a droplet nucleating after this point drops significantly. The high viscosity leads to the flattening out of

the number of uncrystallized droplets after  $\sim 2$  s. By contrast, even when reaching high solute concentrations, the viscosity of aqueous NaCl is never greater than  $10^{-2}$  Pa·s.<sup>43</sup> Hence, the viscosity never impedes nucleation in evaporating aqueous NaCl droplets, and the red line in Figure 1b can be seen to drop to zero when all droplets nucleate at a similar time. Viscosity has been suggested previously to be an important factor in governing the phase behavior of NaNO<sub>3</sub> in mixed-component aerosol: a previous FTIR study of the equilibrium hygroscopic response has shown the presence of a viscous organic solute such as sucrose in a sodium nitrate aerosol droplet reduces the thermodynamic efflorescence RH.<sup>45</sup>

**III.b. Phase Functions of Evaporating Aqueous NaNO<sub>3</sub> Droplets.** If an evaporating droplet nucleates crystals, the particle could show two different types of PF. It could show a crystalline morphology, where there are no regularly spaced fringes from which the CK-EDB software can calculate the radius from and typically the data after this point is noisy. Such a PF generally suggests that the particle is non-homogeneous or nonspherical. Alternatively, the PF could show inclusions, wherein the particle is still relatively spherical in shape, but there are regions of inhomogeneity inside that disrupt the light scattering. There are still interference fringes, but the variation in scattered intensity with angle no longer smoothly decreases with increasing angle and instead shows a rapidly fluctuating intensity profile.

The time-evolving radius profile for an evaporating aqueous NaNO<sub>3</sub> droplet that nucleates at 2.09 s is shown in Figure 2a. The inset shows the particle phase function at two defined times: one prior to crystal nucleation ( $t = 1$  s) and one after crystallization ( $t = 2.3$  s). There is a clear difference in the angularly dependent intensity profiles between the two phase functions. By contrast, Figure 2b shows the time-evolving profile for an aqueous NaNO<sub>3</sub> droplet that nucleates 3 s into the evaporation process. Here the inset shows the PF at three different times. The PF for the droplet that nucleates early (Figure 2a) goes straight from showing a homogeneous spherical morphology (blue points) to a crystalline morphology (red points). However, in Figure 2b the PFs indicate the particle is homogeneous and spherical until  $\sim 3.2$  s when a droplet containing inclusions is detected (yellow points). The radius after 3.2 s remains relatively constant within the uncertainty in the radius retrieval.

The reason that aqueous NaNO<sub>3</sub> droplets nucleate at times later than  $\sim 2$  s into evaporation exhibit a different PF to those that nucleate crystals earlier in the process could be a viscosity-driven effect. If ion-pair formation and nucleation can occur quite soon after solute saturation is reached, there may still be sufficient water present to act as a plasticizer and ensure a level of ion mobility that can support subsequent crystallization throughout the rest of the droplet. The droplet will thus display a PF representative of a completely crystallized particle. However, a droplet that nucleates after 2 s does not retain sufficient water to act as a plasticizer, suppressing internal diffusion within the particle. This can lead to crystal nucleation at multiple unconnected sites within the particle, giving rise to phase functions indicative of the presence of inclusions within the final particle.

**III.c. SEM Images of Dried NaNO<sub>3</sub> Particle Morphologies.** Particles of NaNO<sub>3</sub> dried under the same conditions (0% RH, 293 K) as the data reported in Figure 2 were collected on a glass slide and imaged with scanning electron microscopy (Figure 3a). Two additional samples were

collected from the same drying event as Figure 3a but stored at different RHs prior to SEM imaging to explore the phase (crystalline or amorphous) and morphology of dried NaNO<sub>3</sub> particles. Where the sample in Figure 3a was stored in a 0% RH desiccator following the initial drying but before SEM imaging, the sample in Figure 3b was stored for 7 h in a sealed container at  $60 \pm 2\%$  RH, before being returned to a desiccator prior to the SEM imaging step. In addition, the sample in Figure 3c was stored for 2 h at  $90 \pm 5\%$  RH before being returned to a desiccator prior to imaging.

All dried particles in the sample in Figure 3a were spherical in shape, with wrinkles, cracks, and dimples in the surface of the particles. This can be likely attributed to incomplete dehydration during drying, as typically SEM observation of wet samples under the electron beam leads to collapse, shrinkage, and distortion.<sup>46</sup> The rough surface of these microparticles has been seen in previous studies where aqueous NaNO<sub>3</sub> droplets were dried in a falling column.<sup>42,47</sup> Even though Figure 1b shows that the vast majority of evaporating aqueous NaNO<sub>3</sub> droplets under these conditions would undergo nucleation and crystallization, the dried particles still look spherical. This can be attributed to the high viscosity of the dehydrated NaNO<sub>3</sub> solution at the point of nucleation: a spherical drying droplet is not plasticized sufficiently to arrange to form a regular crystal across the whole particle. The appearance of dried NaNO<sub>3</sub> particles can be compared with that of dried NaCl, produced by evaporating droplets of 20% (w/w) aqueous NaCl in 0% RH N<sub>2</sub> at 318 K (Figures 3d,e). In contrast to the wrinkled, spherical shapes of the NaNO<sub>3</sub> particles, the NaCl particles show complete crystallization, with each particle comprising several connected cubic crystals, with defined edges and smooth faces.

The SEM image of another sample of NaNO<sub>3</sub> particles is shown in Figure 3b. These particles, although dried in an identical way to those in Figure 3a, were stored at  $60 \pm 2\%$  RH after the drying step. Two types of particles can be identified after such a change in the environmental conditions: some dried NaNO<sub>3</sub> particles have clearly absorbed moisture in the higher storage RH conditions and spread out across the glass slide. However, some particles, notably those in the bottom left-hand corner of Figure 3b, remain in a spherical shape similar to those observed in Figure 3a. These particles clearly did not absorb water while stored at 60% RH. From these observations, we can infer that particles were deposited in two phase states, consistent with Figure 1. For the fraction remaining spherical in shape on elevation of RH, we can assume that crystallization occurred on drying; then, a crystalline particle is unable to absorb water at 60% RH and is only able to deliquesce at higher RH (75%). By contrast, the particles observed to absorb water and spread out are unlikely to have crystallized during the initial drying step, forming instead amorphous particles. In the absence of crystallinity, these particles can absorb water at 60% RH.

All of the dried NaNO<sub>3</sub> sample that was stored at  $90 \pm 5\%$  RH prior to SEM imaging dissolved and spread out on the glass slide, as shown in Figure 3c. As 90% RH is higher than the deliquescence RH of NaNO<sub>3</sub>, all particles in this sample could absorb water during the raised RH step, i.e., both the particles that had nucleated crystals and those that had not. Combined, the particle morphologies reported in Figure 3 confirm the interpretation of our kinetics measurements reported in Figure 1 which show the occurrence of NaNO<sub>3</sub>

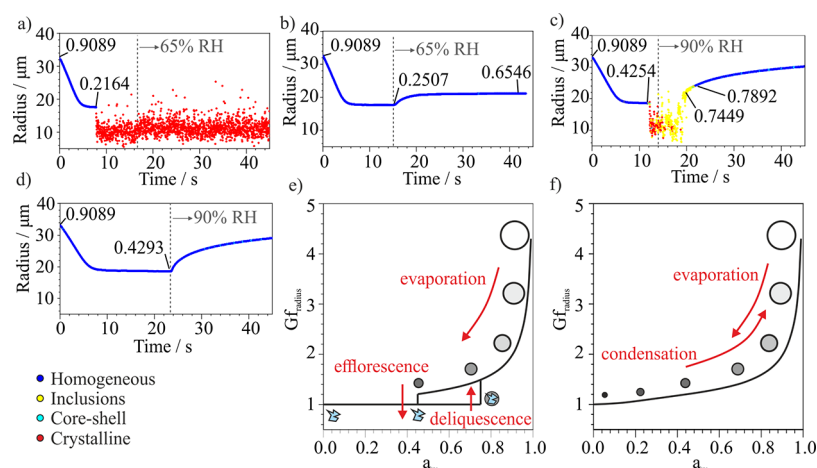


**Figure 4.** Radius evolution of individual droplets dried into RHs lower than the ERH, followed by a rapid switch to a greater RH. In (a) and (c) the droplets nucleate crystals in the initial drying step, whereas in (b) and (d) the droplets equilibrate with the low-RH environment with no crystals nucleated. The RH is switched at the gray line to 90% in (a) and (c) and to 65% in (b) and (d). (e) and (f) show the aerosol phase behavior diagram to demonstrate the dehydration–rehydration steps for droplets that crystallize and those that dry to form amorphous particles, respectively. The color scheme of data points represents the phase state of the aerosol as determined by the elastic light scattering: blue = homogeneous, spherical; red = crystalline, nonspherical; and yellow = spherical with inclusions.

nucleation and crystallization in drying droplets to be variable, with some droplets not appearing to nucleate crystals at all.

In the CK-EDB, the RH of the nitrogen gas passing over a trapped particle can be rapidly changed (over a time scale of  $\sim 0.1$  s) by switching between two gas flows of different humidity. Thus, the RH cycling experiment described for collected samples, observing how dried particles behave when exposed to an increased humidity, can be performed for a single trapped particle. The processing of two aqueous droplets of 20 wt %  $\text{NaNO}_3$ , dried into an RH lower than the ERH and exhibiting crystallization, are shown in Figure 4a,c. When the RH is stepped up to 90% in Figure 4c, the trapped droplet deliquesces, demonstrating that indeed the transition observed at  $\sim 12$  s was efflorescence and the particle in the trap was crystalline (confirmed by the particle phase function). When the RH is stepped up only to 65% in Figure 4a, i.e., below the DRH of 75%, the crystalline particle, inferred from its phase function, does not deliquesce. By contrast, Figures 4b and 4d show two droplets that did not undergo crystallization within the trap when dried to below the ERH, remaining as amorphous particles. In both cases the droplets are observed to reabsorb water when the RH in the trap is stepped up to either 90% or 65%.

The color scheme of the data points in Figure 4 is the same as that used in Figure 2, wherein blue indicates a homogeneous and spherical droplet and red and yellow indicate nucleation, either complete crystallization or in the form of smaller nuclei inclusions, respectively. The calculated water activity at certain time points is indicated, which is estimated from the radius as follows. The mass and dry radius of pure  $\text{NaNO}_3$  in each droplet can be calculated by using the known initial concentration of  $\text{NaNO}_3$  and the initial droplet radius. Thus, for each radial point, a radial growth factor can be retrieved, which relates to a water activity as outlined by the known hygroscopicity of the  $\text{NaNO}_3$  aerosol.<sup>32</sup> The crystalline particle in Figure 4c only becomes an homogeneous liquid droplet above a water activity of 0.75, which is the DRH. Hence, as in Figure 3, we see water uptake by amorphous particles at all RHs but only water uptake above the DRH for crystalline particles. This also serves as further evidence that the light

scattering seen in evaporating  $\text{NaNO}_3$  droplets can be used to define the time at which nucleation occurs.

**III.d. Observing Variable Nucleation Behavior in a Single Droplet.** Nucleation can occur through one of two mechanisms: homogeneous or heterogeneous. Typically, at low levels of supersaturation homogeneous nucleation in inorganic salt solutions is a rare event and occurs over very long time scales. Heterogeneous nucleation is caused by the presence of surfaces, dust, or impurities and is often the dominant route to crystallization as it can occur at a lower degree of solute supersaturation. An aerosol droplet on the order of micrometers in radius has the absence of any surface and a low probability of dust or impurity being present; hence, very high degrees of solute supersaturation can be reached without any heterogeneous nucleation taking place (see Table 1). Hence, aerosol droplets can serve as a contactless confined

**Table 1. Solute Concentration and Degree of Supersaturation for a  $\text{NaNO}_3$  Droplet That Has Equilibrated to a Range of RHs and Not Yet Nucleated Crystals, Calculated in Terms of Molarity**

RH (%)	concentration <sup>a</sup> ( $\text{g L}^{-1}$ )	supersaturation at 293 K
40	1480	2.60
30	1650	2.89
25	1740	3.05
20	1840	3.23
15	1940	3.40

<sup>a</sup>Concentration at solubility limit (0.465 MFS) =  $570 \text{ g L}^{-1}$ .

volume in which to probe homogeneous nucleation processes. The nucleation observed in an aerosol droplet is directly a result of the stochastic process of homogeneous nucleation: the random and rare event that ion pairs form and arrange into a crystal nucleus.

To demonstrate that the differences in the nucleation and crystallization behavior observed within the population of  $\text{NaNO}_3$  droplets are not caused by the presence of impurities or dust present in only a fraction of the particles, a single aqueous  $\text{NaNO}_3$  droplet of initial concentration 20% solute

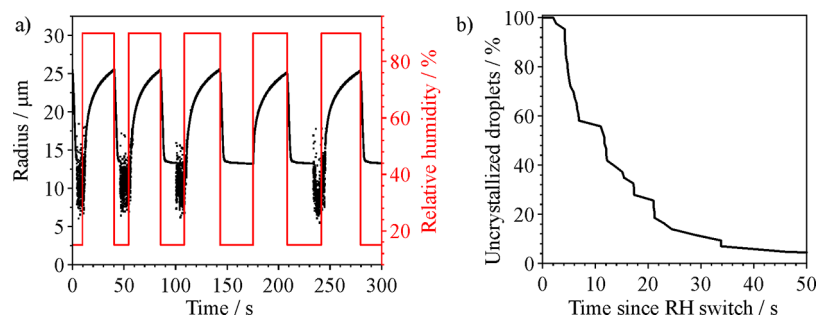


**Figure 5.** (a) Radius evolution of a single aqueous  $\text{NaNO}_3$  droplet (20% w/w) as the RH is continuously stepped up to 90% or down to 18% in six examples of a series of 40 drying events all with the same droplet. (b) Distribution of the time taken for the droplet to nucleate crystals for every drying event.

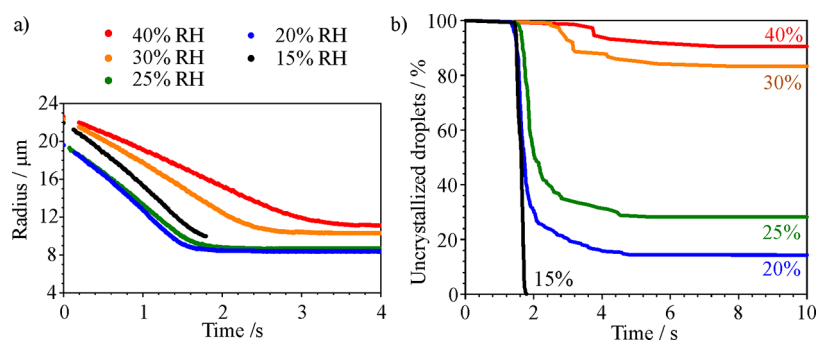


**Figure 6.** (a) Evolution of droplet radius for  $\text{NaNO}_3$  droplets (12.5% w/w) evaporating in the CK-EDB at 293 K at varying RHs. (b) Distribution of nucleation events with time for the different RHs, for a population of 75+ droplets for each data set.

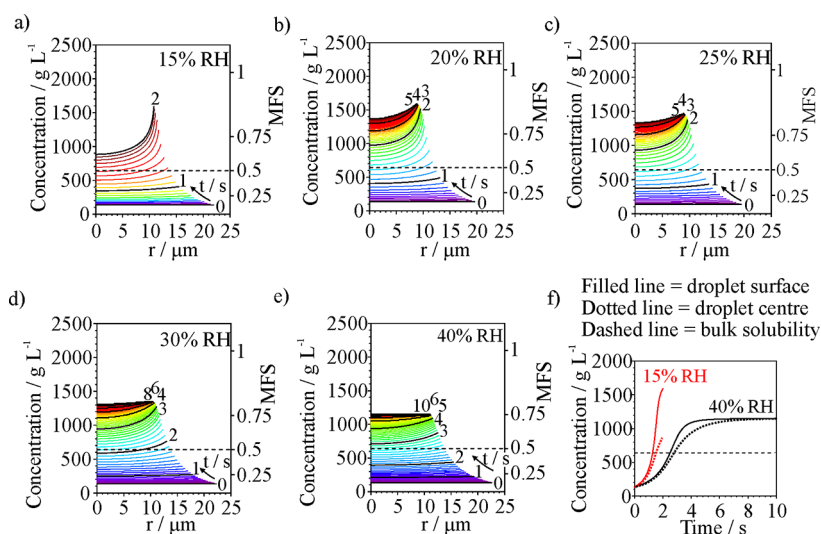


**Figure 7.** (a–e) Modeling results of the time-dependent internal solute concentration profiles along the cross section of an aqueous  $\text{NaNO}_3$  droplet in Figure 6a as it evaporates into varying RHs, where  $r$  is the distance from the droplet center. The data are plotted as a molarity concentration as well as a mass fraction of solution (MFS). The data are plotted every 0.1 s, with the time indicated every 1 s. The black dotted line shows the  $\text{NaNO}_3$  bulk solubility limit at 293 K. (f) Comparison between the time-dependent concentration of  $\text{NaNO}_3$  at the droplet surface (filled) and the droplet center (dotted) for an aqueous  $\text{NaNO}_3$  droplet drying at 15% and 40% RH.

weight was repeatedly evaporated in a series of RH-switching experiments. First, the droplet is evaporated into 18% RH (below the ERH for  $\text{NaNO}_3$ ) and retained for a period of 30 s to see whether nucleation and crystallization occur. Following crystallization (determined from monitoring changes in the phase function), or at the end of a 30 s time period over which no phase change was observed, the RH was rapidly switched to an RH of 90% (above the DRH for  $\text{NaNO}_3$ ) by using the CK-EDB dual gas flows. The particle, whether crystalline or

amorphous, absorbed water from the gas phase and grew in radius. Once the droplet re-equilibrated to its initial starting size, the gas flow was switched once more to 18% RH, and the evaporation of the droplet was monitored. This process was repeated many times, with the resulting radius vs time profile shown in black in Figure 5a; the RH (as a function of time) is shown in red, clearly denoting the switching of the gas flows. The time at which nucleation and crystallization occurred is

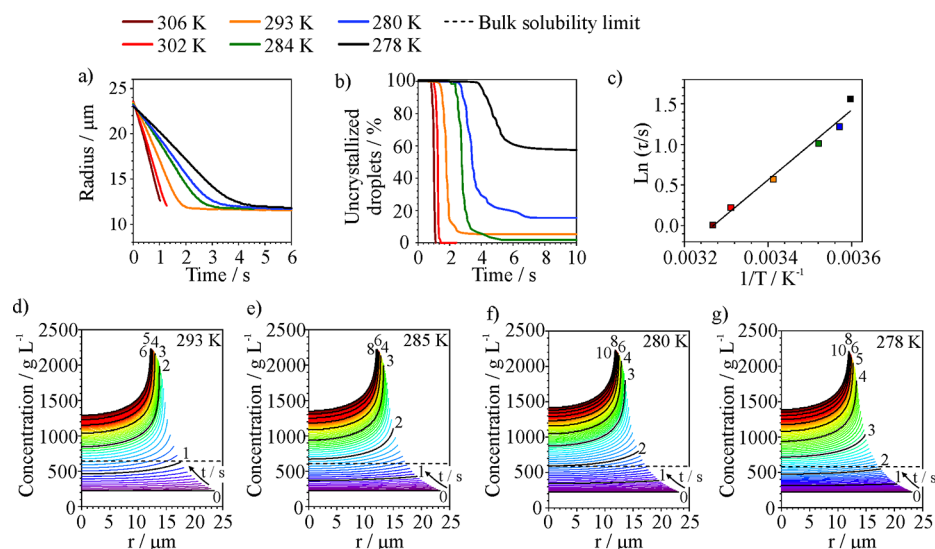


**Figure 8.** (a) Radius evolution of 20% NaNO<sub>3</sub> droplets evaporating into 0% RH at varying gas-phase temperatures in the CK-EDB. (b) The time-dependent distribution of nucleation events across a population of 50+ droplets for each data set. (c–f) Modeled concentration profiles across a droplet cross section for the drying events 278–293 K in (a), where  $r$  is the distance from the droplet center. The data are plotted every 0.1 s, with the time indicated every 1 s.

evident from the large increase in noise in the reported droplet radius.

The data in Figure 5a show that the same aqueous NaNO<sub>3</sub> droplet, held continuously in the trap for multiple RH cycles, exhibited a different efflorescence time each time the droplet is dried. On some occasions the droplet did not effloresce during the 30 s time window allocated for the RH switch, while in other cycles it nucleated in only 2 s. Figure 5b shows the time-dependent decay (over all the evaporation–condensation cycles) for the liquid droplet as a function of time. This figure demonstrates that the variation in nucleation time during the evaporation of many droplets in a series cannot be caused by different droplets containing varying amounts of impurities or dust because here each drying event has the same exact mass of NaNO<sub>3</sub> with the same potential for impurities. We can conclude that the variability observed in NaNO<sub>3</sub> nucleation times is dominated by the stochastic nature of crystal nucleation.

**III.e. Variation in Nucleation Propensity for NaNO<sub>3</sub> at Different RHs.** The droplet-to-droplet variation in nucleation time observed in NaNO<sub>3</sub> droplets can be observed across a range of experimental conditions. Figure 6a reports the crystallizing fraction of evaporating droplets into different RHs. It must be noted that the initial droplet size for the 20% and 25% RH data sets is lower; a version of this figure with the data normalized for the initial starting radius allowing comparison of the evaporation rates is presented in the Supporting Information (Figure S5). The time dependence for the nucleating fraction of droplets across a large population (70+ droplets in each case) is shown in Figure 6b. As droplets evaporate at lower RHs, the percentage of droplets that nucleate in a 10 s experimental window is seen to increase, and crystallization is observed to occur at earlier times. The reasons behind this are evident from the modeled concentration profiles within the evaporating droplet, as shown in Figure 7. The NaNO<sub>3</sub> concentration at the surface rises more quickly when drying into lower RH.

The general trend in the concentration profiles shows a steep rise in surface solute concentration with time, which

peaks at a maximum value that increases as the evaporation occurs in lower RH. At 15% RH, the maximum surface concentration predicted by the model before crystal nucleation occurs is 1590 g L<sup>-1</sup>, or 18.7 M, which corresponds to a degree of supersaturation in molarity space of 2.48. All droplets nucleate crystals by the time that this maximum in supersaturation is reached. It is likely that nucleation occurs at the surface, where there is a very steep concentration gradient, shown by the model. For a RH of 20% and higher, a fraction of droplets do not nucleate crystals even when the peak in solute concentration is reached. The droplets remaining then have a concentration gradient that levels out across the droplet as bulk diffusional mixing outweighs the evaporative flux of water leaving the surface. At long time scales, these droplets would eventually achieve a radially uniform solute concentration, with a higher equilibrated solute concentration that is greater for the lower RHs. A higher solute concentration leads to a higher chemical potential and greater drive for crystal nucleation. The degree of supersaturation in terms of the molarity calculated by using the E-AIM model can be as high as 3.48 for an uncrystallized droplet that has equilibrated at 15%, as shown in Table 1.<sup>48</sup> The time evolution in the NaNO<sub>3</sub> concentration at the surface and at the center for droplets evaporating into 15% and 40% RH is compared in Figure 7f. A very large degree of surface enrichment is inferred to occur at a drying RH of 15% (with a large disparity between the center and the surface). However, for drying at 40% RH, an enriched surface reaches a limiting maximum solute concentration, and the evaporation rate then reduces, leading once more to a homogeneous droplet after 10 s.

**III.f. Variation in Nucleation Propensity at Different Temperatures.** As part of the exponent in eq 2, the temperature is an influential factor in classical nucleation theory, acting to increase the nucleation rate with increasing temperature with all other quantities being equal. The increase in temperature leads to a greater degree of thermal motion of the ions, leading to a greater chance for the necessary interactions to occur that lead to nucleation. Indeed, with an increasing gas phase temperature, the likelihood of forming a

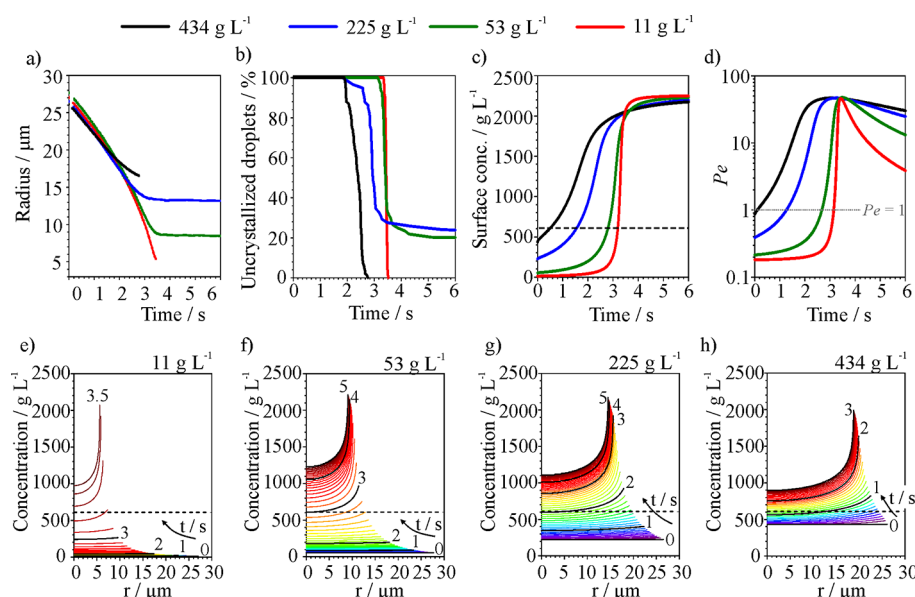


**Figure 9.** (a) Radius evolution of  $\text{NaNO}_3$  droplets evaporating into 0% RH at 284.5 K with varying starting concentrations. (b) Time-dependent distribution of nucleation events across a population of 50+ droplets for each data set. (c) Model results of the time-dependent surface concentration. (d) Time-dependent Péclet number. (e–h) Modeled concentration profiles across a droplet cross section for the drying events in (a), where  $r$  is the distance from the droplet center. The data are plotted every 0.1 s, with the time indicated every 1 s. The dashed line indicates the bulk solubility limit.

crystal nucleus in an evaporating  $\text{NaNO}_3$  droplet increases, as shown in Figure 8b. The proportion of droplets remaining uncrystallized falls from 100% to 0% within only a few hundred milliseconds at 306 K; at 278 K, the time for droplets to nucleate crystals spreads over several seconds, and the majority of droplets do not display nucleation within the experimental window. At colder temperatures, the droplet evaporation rate decreases, as shown in Figure 8a, which leads to a greater time available for nucleation. However, the nucleation rate is lower at 278 K, and even with the slower evaporation rate, the droplet loses all of its water through evaporation before contact-ion pairs have time to arrange into a crystal nucleus.

The distribution of nucleation events in evaporating  $\text{NaNO}_3$  droplets at varying temperatures in Figure 8b can be converted into a half-life,  $\tau$ , of remaining uncrystallized droplets.  $\tau$  is taken as the time taken for half of the droplets in each data set to nucleate crystals, out of those that do nucleate within the experimental window of 10 s.  $\tau$  relates to the inverse of the nucleation rate, so according to eq 2, plotting  $\ln(\tau)$  against  $1/T$  where  $T$  is the gas-phase temperature yields a straight line with gradient  $-\Delta G^*/k_B$ . This is shown in Figure 8c, wherein the gradient of the straight-line fit (black line) is  $4300 \pm 300$  K. This enables the calculation of the Gibbs free energy barrier to nucleation,  $\Delta G^*$ , as  $36 \pm 3$  kJ mol $^{-1}$ . Fitting a straight line to this plot validates the Arrhenius form of the nucleation rate of  $\text{NaNO}_3$  in eq 2, showing that the nucleation is an activated process.

The modeled concentration profiles in evaporating  $\text{NaNO}_3$  droplets (20% w/w) in 0% RH at 293, 285, 280, and 278 K are reported in Figures 8d–g, respectively. The maximum solute concentrations achieved at the surface of the droplets are similar because the droplets are all evaporating into dry air and reach approximately the same equilibrated radius, as shown in Figure 8a. This demonstrates that the  $\text{NaNO}_3$  nucleation rate is strongly temperature dependent and is not just dependent on the degree of supersaturation reached in a droplet.

**III.g. Variation in Nucleation Propensity for Different Starting Concentrations.** The concentration dependence upon the nucleation propensity of aqueous  $\text{NaNO}_3$  is demonstrated in Figure 9, where the initial concentration was varied for different populations of droplets evaporating at 285 K and 0% RH.

The chance of forming a crystal nucleus varies as a function of time in each case. The evaporation rate of the lower solute concentration droplets is slightly faster, as shown in Figure 9a, due to the greater vapor pressure of water arising from a lower solute activity. Hence, the droplets in these measurements would be exposed to a greater degree of evaporative cooling. Liquid droplets of  $\sim 25$   $\mu\text{m}$  in radius evaporating into dry air have been shown to fall to several tens of degrees colder in temperature than the surrounding gas temperature.<sup>49</sup> Thus, the trend in nucleation propensity reported in Figure 9 is a result of the interplay between nucleation rate at the droplet temperature and the time available for crystals to form. The modeled concentration profiles of the droplets evaporating with different initial starting concentration are shown in Figures 9e–h. For the droplets with the lowest initial concentration droplet (Figure 9e), there is little time available for crystallization because the whole droplet is far below the bulk solubility limit until quite late into evaporation. When eventually it does surpass the solubility limit, the solute concentration at the droplet surface is very high due to the huge degree of enrichment from the rapid evaporation, and nucleation occurs rapidly. Conversely, a slightly higher initial concentration of 50 or 200 g L $^{-1}$  leads to a more gradual degree of surface enrichment during evaporation, and some droplets nucleate crystals before the surface of the droplet becomes too viscous.

A droplet starting at a concentration of 434 g L $^{-1}$  is already quite close to the  $\text{NaNO}_3$  bulk solubility limit of 642 g L $^{-1}$  and evaporates at the slowest rate. When it passes the solubility limit, it has the longest crystallization window of all

evaporation conditions reported in Figure 9. This is demonstrated in Figure 9c, where the black line shows the evolution of the surface concentration of the droplet with a starting concentration of 434 g L<sup>-1</sup>. The solubility limit is surpassed at the surface very rapidly, and hence, there is a long time window for crystals to nucleate before the drying is complete. This argument does not explain why the droplets starting with the lowest concentration (11 g L<sup>-1</sup>) nucleate very rapidly and reproducibly despite the smallest time window available for crystal nucleation. The nucleation behavior of droplets of this starting composition may be related to how rapidly the surface concentration rises at the end of evaporation in Figure 9c. The evaporation rates (Figure 9a) can be compared to the rate of diffusional mixing at the droplet surface, from the surface concentration (Figure 9c), by using the Péclet number ( $Pe$ ):<sup>50</sup>

$$Pe = \frac{\kappa}{D_{\text{eff}}} \quad (7)$$

where  $\kappa$  is the evaporation rate ( $dr^2/dt$ ) and  $D_{\text{eff}}$  is the effective binary diffusion coefficient of aqueous NaNO<sub>3</sub> at the droplet surface. The time-dependent  $Pe$  for the evaporation data sets in Figure 9a are shown in panel d. A  $Pe$  greater than 1 represents when the evaporation rate is faster than the rate of diffusional mixing. Thus,  $Pe > 1$  indicates that the droplet may become enriched with solute at the surface and that the viscosity is the limiting factor in the mass transport during evaporation. For all initial NaNO<sub>3</sub> concentrations, the  $Pe$  increases to a similar maximum value (Figure 9d), but the time window for which the high  $Pe$  is maintained, where the evaporation rate is much greater than the diffusional mixing rate, is longer for the higher starting concentration.

Overall, the data in Figure 9 demonstrate how variable the nucleation behavior for evaporating aqueous NaNO<sub>3</sub> droplets can be depending on the initial conditions. By only varying the starting concentration, we show that the ratio between crystalline and amorphous particles formed during drying can be tuned. These data can be used to infer the absolute values of the temperature- and concentration-dependent nucleation rate for aqueous NaNO<sub>3</sub>, which are discussed in more detail in another publication.<sup>38</sup> The ability to model the interplay between the crystal nucleation rate and the time available for crystallization would be very valuable for spray drying models of viscous droplet evaporation.

## IV. CONCLUSIONS

Inorganic aerosol solution droplets typically crystallize when the surrounding relative humidity (RH) is reduced, and the threshold RH below which crystallization is observed is often described as the efflorescence RH. Although there have been multiple studies on the hygroscopicity of NaNO<sub>3</sub> aerosol particles, there remains an absence of agreement on the value of the ERH, and there has been limited work on the kinetics of the nucleation rate. Using the comparative-kinetics electrodynamic balance, we can isolate one single liquid droplet of aqueous NaNO<sub>3</sub> at a time and study the evaporation kinetics and nucleation behavior of a population of many hundreds of identical droplets. Where NaCl solutions show a highly reproducible nucleation behavior with very little variation in the time that different droplets nucleate crystals when a specific supersaturation is reached, NaNO<sub>3</sub> droplets in a series show a broad distribution in the time that crystals nucleate. Even when evaporating in 0% RH, some NaNO<sub>3</sub> droplets do not nucleate

crystals in the time window taken for the water to evaporate, leaving an amorphous dry particle. The distribution of nucleation time is dependent upon the drying conditions (temperature, RH, and initial NaNO<sub>3</sub> concentration). We believe that the reason behind this interesting nucleation behavior is that the viscosity of NaNO<sub>3</sub> solutions can increase in 4–5 orders of magnitude as the solute concentration rises, which in turn reduces the nucleation rate at very high supersaturations. There is a competition between nucleation rate and the time available for crystallization (the drying time), and this interplay controls the ratio of amorphous or crystallized dry particles. This data set of nucleation rates under different conditions would be useful for validating models of nucleation rates of viscous droplet drying, which is important for product control in spray drying.

## ■ ASSOCIATED CONTENT

### Supporting Information

The Supporting Information is available free of charge at <https://pubs.acs.org/doi/10.1021/acs.jpbc.0c04079>.

Examples of the elastic light scattering patterns of the laser light by droplets exhibiting different morphologies; a schematic diagram of the setup of the falling droplet column instrument; a comparison between the experimentally obtained droplet radii during evaporation and the fitted model; the viscosity of aqueous NaNO<sub>3</sub> as a function of solute concentration and temperature; and the binary diffusion coefficient of aqueous NaNO<sub>3</sub> solutions as implemented in the model presented in this work, normalized evaporation rates of NaNO<sub>3</sub> droplets under varying RHs (PDF)

## ■ AUTHOR INFORMATION

### Corresponding Author

F. K. A. Gregson – School of Chemistry, University of Bristol, Bristol BS8 1TS, U.K.; [orcid.org/0000-0002-8516-0796](https://orcid.org/0000-0002-8516-0796); Email: [florence.gregson@bristol.ac.uk](mailto:florence.gregson@bristol.ac.uk)

### Authors

J. F. Robinson – School of Physics, University of Bristol, Bristol BS8 1TS, U.K.

R. E. H. Miles – School of Chemistry, University of Bristol, Bristol BS8 1TS, U.K.

C. P. Royall – School of Chemistry and School of Physics, University of Bristol, Bristol BS8 1TS, U.K.

J. P. Reid – School of Chemistry, University of Bristol, Bristol BS8 1TS, U.K.; [orcid.org/0000-0001-6022-1778](https://orcid.org/0000-0001-6022-1778)

Complete contact information is available at:

<https://pubs.acs.org/doi/10.1021/acs.jpbc.0c04079>

### Notes

The authors declare no competing financial interest.

## ■ ACKNOWLEDGMENTS

The authors acknowledge the support from the Engineering and Physical Sciences Research Council under Grant Code EP/N025245/1.

## ■ REFERENCES

(1) Carver, K. M.; Snyder, R. C. Unexpected Polymorphism and Unique Particle Morphologies from Monodisperse Droplet Evaporation. *Ind. Eng. Chem. Res.* **2012**, *51*, 15720–15728.

- (2) Lintingre, E.; Lequeux, F.; Talini, L.; Tsapis, N. Control of Particle Morphology in the Spray Drying of Colloidal Suspensions. *Soft Matter* **2016**, *12*, 7435–7444.
- (3) Ivey, J. W.; Bhambri, P.; Church, T. K.; Lewis, D. A.; Vehring, R. Experimental Investigations of Particle Formation from Propellant and Solvent Droplets Using a Monodisperse Spray Dryer. *Aerosol Sci. Technol.* **2018**, *52*, 702–716.
- (4) You, X.; Zhou, Z.; Liao, Z.; Che, L.; Chen, X. D.; Wu, W. D.; Woo, M.; Selomulya, C. Dairy Milk Particles Made with a Mono-Disperse Droplet Spray Dryer (MDDSD) Investigated for the Effect of Fat. *Drying Technol.* **2014**, *32*, 528–542.
- (5) Lin, R.; Liu, W.; Woo, M. W.; Chen, X. D.; Selomulya, C. On the Formation of “Coral-like” Spherical  $\alpha$ -Glycine Crystalline Particles. *Powder Technol.* **2015**, *279*, 310–316.
- (6) Yu, L.; Ng, K. Glycine Crystallization during Spray Drying: The PH Effect on Salt and Polymorphic Forms. *J. Pharm. Sci.* **2002**, *91*, 2367–2375.
- (7) Dubbini, A.; Censi, R.; Martena, V.; Hoti, E.; Ricciutelli, M.; Malaj, L.; Di Martino, P. Influence of PH and Method of Crystallization on the Solid Physical Form of Indomethacin. *Int. J. Pharm.* **2014**, *473*, 536–544.
- (8) Nandiyanto, A. B. D.; Okuyama, K. Progress in Developing Spray-Drying Methods for the Production of Controlled Morphology Particles: From the Nanometer to Submicrometer Size Ranges. *Adv. Powder Technol.* **2011**, *22*, 1–19.
- (9) Xia, B.; Lenggoro, I. W.; Okuyama, K. Synthesis of CeO<sub>2</sub> Nanoparticles by Salt-Assisted Ultrasonic Aerosol Decomposition. *J. Mater. Chem.* **2001**, *11*, 2925–2927.
- (10) Lyu, F.; Liu, J. J.; Zhang, Y.; Wang, X. Z. Combined Control of Morphology and Polymorph in Spray Drying of Mannitol for Dry Powder Inhalation. *J. Cryst. Growth* **2017**, *467*, 155–161.
- (11) Amstad, E.; Spaepen, F.; Weitz, D. A. Stabilization of the Amorphous Structure of Spray-Dried Drug Nanoparticles. *J. Phys. Chem. B* **2016**, *120*, 9161–9165.
- (12) Brough, C.; Williams, R. O. Amorphous Solid Dispersions and Nano-Crystal Technologies for Poorly Water-Soluble Drug Delivery. *Int. J. Pharm.* **2013**, *453*, 157–166.
- (13) Vehring, R.; Foss, W. R.; Lechuga-Ballesteros, D. Particle Formation in Spray Drying. *J. Aerosol Sci.* **2007**, *38*, 728–746.
- (14) Shakiba, S.; Mansouri, S.; Selomulya, C.; Woo, M. W. The Role of the Intermediate Stage of Drying on Particle In-Situ Crystallization in Spray Dryers. *Powder Technol.* **2018**, *323*, 357–366.
- (15) Costantino, H. R.; Andya, J. D.; Nguyen, P.-A.; Dasovich, N.; Sweeney, T. D.; Shire, S. J.; Hsu, C. C.; Maa, Y.-F. Effect of Mannitol Crystallization on the Stability and Aerosol Performance of a Spray-Dried Pharmaceutical Protein, Recombinant Humanized Anti-IgE Monoclonal Antibody. *J. Pharm. Sci.* **1998**, *87*, 1406–1411.
- (16) Ali, M.; Mahmud, T.; Heggs, P. J.; Ghadiri, M.; Bayly, A.; Ahmadian, H.; Martin de Juan, L. CFD Modeling of a Pilot-Scale Countercurrent Spray Drying Tower for the Manufacture of Detergent Powder. *Drying Technol.* **2017**, *35*, 281–299.
- (17) Wawrzyniak, P.; Podyma, M.; Zbicinski, I.; Bartzczak, Z.; Rabaeva, J. Modeling of Air Flow in an Industrial Countercurrent Spray-Drying Tower. *Drying Technol.* **2012**, *30*, 217–224.
- (18) Lin, R.; Woo, M. W.; Fu, N.; Selomulya, C.; Chen, X. D. In Situ Observation of Taurine Crystallization via Single Droplet Drying. *Drying Technol.* **2013**, *31*, 1553–1561.
- (19) Sear, R. P. Quantitative Studies of Crystal Nucleation at Constant Supersaturation: Experimental Data and Models. *CrystEngComm* **2014**, *16*, 6506–6522.
- (20) Vekilov, P. G. Nucleation of Crystals in Solution. *AIP Conf. Proc.* **2010**, *1270*, 60–77.
- (21) Gibbs, J. W. Equilibrium of Heterogeneous Substances. *Trans. Connect. Acad. Arts Sci.* **1876**, *3*, 108–248.
- (22) Gibbs, J. W. On the Equilibrium of Heterogeneous Substances. *Trans. Connect. Acad. Arts Sci.* **1878**, *3*, 343–524.
- (23) He, G.; Bhamidi, V.; Tan, R. B. H.; Kenis, P. J. A.; Zukoski, C. F. Determination of Critical Supersaturation from Microdroplet Evaporation Experiments. *Cryst. Growth Des.* **2006**, *6*, 1175–1180.
- (24) Karthika, S.; Radhakrishnan, T. K.; Kalaichelvi, P. A Review of Classical and Nonclassical Nucleation Theories. *Cryst. Growth Des.* **2016**, *16*, 6663–6681.
- (25) Krieger, U. K.; Marcolli, C.; Reid, J. P. Exploring the Complexity of Aerosol Particle Properties and Processes Using Single Particle Techniques. *Chem. Soc. Rev.* **2012**, *41*, 6631–6662.
- (26) Gregson, F. K. A.; Robinson, J. F.; Miles, R. E. H.; Royall, C. P.; Reid, J. P. Drying Kinetics of Salt Solution Droplets: Water Evaporation Rates and Crystallization. *J. Phys. Chem. B* **2019**, *123*, 266–276.
- (27) Baldelli, A.; Power, R. M.; Miles, R. E. H.; Reid, J. P.; Vehring, R. Effect of Crystallization Kinetics on the Properties of Spray Dried Microparticles. *Aerosol Sci. Technol.* **2016**, *50*, 693–704.
- (28) Rovelli, G.; Miles, R. E. H.; Reid, J. P.; Clegg, S. L. Accurate Measurements of Aerosol Hygroscopic Growth over a Wide Range in Relative Humidity. *J. Phys. Chem. A* **2016**, *120*, 4376–4388.
- (29) Wexler, A. S.; Clegg, S. L. Atmospheric Aerosol Models for Systems Including the Ions H<sup>+</sup>, NH<sub>4</sub><sup>+</sup>, Na<sup>+</sup>, SO<sub>4</sub><sup>2-</sup>, NO<sub>3</sub><sup>-</sup>, Cl<sup>-</sup>, Br<sup>-</sup> and H<sub>2</sub>O. *J. Geophys. Res.* **2002**, *107*, 4207–4221.
- (30) CRC Handbook of Chemistry and Physics; Rumble, J. R., Ed.; CRC Press: Boca Raton, FL.
- (31) Ghorai, S.; Tivanski, A. V. Hygroscopic Behavior of Individual Submicrometer Particles Studied by X-Ray Spectromicroscopy. *Anal. Chem.* **2010**, *82*, 9289–9298.
- (32) Tang, I. N.; Munkelwitz, H. R. Water Activities, Densities, and Refractive Indices of Aqueous Sulfates and Sodium Nitrate Droplets of Atmospheric Importance. *J. Geophys. Res.* **1994**, *99*, 18801–18808.
- (33) Lee, M.-J.; Jung, H.-J.; Eom, H.-J.; Maskey, S.; Kim, H. K.; Ro, C.-U. Hygroscopic Behavior of Individual NaNO<sub>3</sub> Particles. *Atmos. Chem. Phys. Discuss.* **2011**, *11*, 23203–23229.
- (34) Davies, J. F.; Haddrell, A. E.; Rickards, A. M. J.; Reid, J. P. Simultaneous Analysis of the Equilibrium Hygroscopicity and Water Transport Kinetics of Liquid Aerosol. *Anal. Chem.* **2013**, *85*, 5819–5826.
- (35) Haddrell, A.; Rovelli, G.; Lewis, D.; Church, T.; Reid, J. P. Identifying Time-Dependent Changes in the Morphology of an Individual Aerosol Particle from Their Light Scattering Patterns. *Aerosol Sci. Technol.* **2019**, *53*, 1334–1351.
- (36) Olsen, A. P.; Flagan, R. C.; Kornfield, J. A. Single-Particle Levitation System for Automated Study of Homogeneous Solute Nucleation. *Rev. Sci. Instrum.* **2006**, *77*, 073901–073908.
- (37) Brandel, C.; ter Horst, J. H. Measuring Induction Times and Crystal Nucleation Rates. *Faraday Discuss.* **2015**, *179*, 199–214.
- (38) Robinson, J. F.; Gregson, F. K. A.; Miles, R. E. H.; Reid, J. P.; Royall, C. P. Drying Kinetics and Nucleation in Evaporating Sodium Nitrate Aerosols. *J. Chem. Phys.* **2020**, *152*, No. 074503.
- (39) Slattery, J. C. *Advanced Transport Phenomena*; Cambridge University Press: Cambridge, UK, 1999.
- (40) Sugiharto, S.; Lewis, T. M.; Moorhouse, A. J.; Schofield, P. R.; Barry, P. H. Anion-Cation Permeability Correlates with Hydrated Counterion Size in Glycine Receptor Channels. *Biophys. J.* **2008**, *95*, 4698–4715.
- (41) Sata, T. Studies on Anion Exchange Membranes Having Permselectivity for Specific Anions in Electrodialysis — Effect of Hydrophilicity of Anion Exchange Membranes on Permselectivity of Anions. *J. Membr. Sci.* **2000**, *167*, 1–31.
- (42) Baldelli, A.; Vehring, R. Control of the Radial Distribution of Chemical Components in Spray Dried Crystalline Microparticles. *Aerosol Sci. Technol.* **2016**, *50*, 1130–1142.
- (43) Power, R. M.; Simpson, S. H.; Reid, J. P.; Hudson, A. J. The Transition from Liquid to Solid-like Behaviour in Ultrahigh Viscosity Aerosol Particles. *Chem. Sci.* **2013**, *4*, 2597–2604.
- (44) Taffs, J.; Williams, S. R.; Tanaka, H.; Royall, C. P. Structure and Kinetics in the Freezing of Nearly Hard Spheres. *Soft Matter* **2013**, *9*, 297–305.
- (45) Ji, Z.; Zhang, Y.; Pang, S.; Zhang, Y. Crystal Nucleation and Crystal Growth and Mass Transfer in Internally Mixed Sucrose/NaNO<sub>3</sub> Particles. *J. Phys. Chem. A* **2017**, *121*, 7968–7975.

(46) Golding, C. G.; Lamboo, L. L.; Beniac, D. R.; Booth, T. F. The Scanning Electron Microscope in Microbiology and Diagnosis of Infectious Disease. *Sci. Rep.* **2016**, *6*, 26516.

(47) Baldelli, A.; Vehring, R. Analysis of Cohesion Forces between Monodisperse Microparticles with Rough Surfaces. *Colloids Surf., A* **2016**, *506*, 179–189.

(48) Clegg, S. L.; Brimblecombe, P.; Wexler, A. S. Thermodynamic Model of the System  $\text{H}^+$  -  $\text{NH}_4^+$  -  $\text{Na}^+$  -  $\text{SO}_4^{2-}$  -  $\text{NO}_3^-$  -  $\text{Cl}^-$  -  $\text{H}_2\text{O}$  at 298.15 K. *J. Phys. Chem. A* **1998**, *102*, 2155–2171.

(49) Gregson, F. K. A.; Ordoubadi, M.; Miles, R. E. H.; Haddrell, A.; Barona, D.; Lewis, D.; Church, T.; Vehring, R.; Reid, J. P. Studies of Competing Evaporation Rates of Multiple Volatile Components from a Single Binary-Component Aerosol Droplet. *Phys. Chem. Chem. Phys.* **2019**, *21*, 9709–9719.

(50) Vehring, R. Pharmaceutical Particle Engineering via Spray Drying. *Pharm. Res.* **2008**, *25*, 999–1022.